THE JOURNAL OF PHYSICAL CHEMISTRY B

ARTICLE

pubs.acs.org/JPCB

Dynamic Crystallization Kinetics and Nucleation Parameters of a New Generation of Nanocomposites Based on Isotactic Polypropylene and MoS_2 Inorganic Nanotubes

Mohammed Naffakh,*[,†] Maja Remškar,[‡,§] Carlos Marco,[†] and Marián A. Gómez-Fatou[†]

[†]Departamento de Física e Ingeniería de Polímeros, Instituto de Ciencia y Tecnología de Polímeros, CSIC, c/Juan de la Cierva, 3, 28006, Madrid, Spain

[‡]Jožef Stefan Institute, Jamona 39, SI-1000 Ljubljana, Slovenia

[§]Centre of Excellence PoliMat, Tehnoloski Park 24, SI-1000 Ljubljana, Slovenia

ABSTRACT: Differential scanning calorimetry (DSC) and time-resolved synchrotron X-ray diffraction have been used to investigate the dynamic crystallization behavior and crystalline structure of novel nanocomposites based on isotactic polypropylene (iPP) and molybdenum disulfide inorganic nanotubes (INT-MoS_2). The influence of the INT-MoS_2 content and different cooling rates on the crystallization behavior has been studied. The crystallization exothermic peak shifted to higher temperature, and the overall crystallization time was reduced by increasing the INT-MoS_2. The dynamic crystallization kinetics was analyzed using the Ozawa−Avrami method, which was successful in describing the dynamic crystallization behavior of these new nanocomposites. On the other hand, study of the nucleation activity using the Dobreva method revealed that the INT-MoS_2 had an efficient nucleation effect on the monoclinic crystal form of iPP. Moreover, this effect was corroborated by the results of the crystallization activation energy, calculated using Kissinger and Takhor methods, which also confirmed the fact that the addition of INT-MoS_2 made the molecular chains easier to crystallize and increased the crystallization rate of iPP.

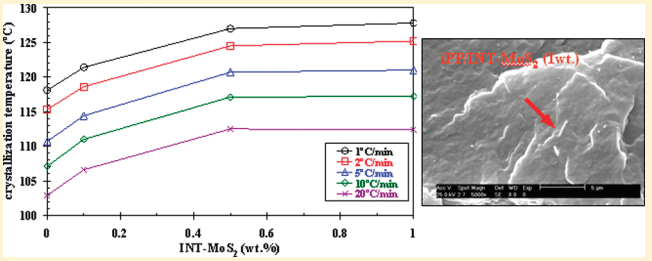

1. INTRODUCTION

The discovery of carbon fullerenes by Kroto, Smalley, and Curl[1] in 1985 and later of carbon nanotubes by Iijima in 1991[2] served as a turning point in the exploration of the potential of these nanostructures. The development of these nanostructures is not limited to carbon, and it was soon recognized that layered metal dichalcogenides such as WS_2 and MoS_2 could also form this genuine property. The first synthesis of such nanophases was reported by Tenne in 1992 and 1993, respectively,[3,4] leading to the birth of a new field of inorganic chemistry, that is, one dealing with polyhedral (closed hollow) nanostructures. Since then, the number of articles related to the successful growth of inorganic nanotubes (INT) and fullerene-like (IF) nanoparticles from inorganic compounds with layered two-dimensional structures has increased rapidly, showing the importance of this field for nanotechnology.[5,6] Various potential applications have been proposed for these nanophases due to their excellent solid lubrication behavior, suggesting many applications in, for example, the automotive and aerospace industries, home appliances, and recently for medical technology.[6] In particular, the revolutionary properties of inorganic fullerene-like nanoparticles (e.g., tungsten disulfide, IF-WS_2), such as high modulus and low friction coefficient, attributed to their small size, closed structure, and chemical inertness, make them potential candidates to improve the thermal, mechanical, and tribological properties of thermoplastic polymers, as has been shown for isotactic polypropylene (iPP),[7,8] polyphenylene sulfide (PPS),[9−11] and PEEK[12] produced via melt blending, without using modifiers or surfactants. Other potential applications, in catalysis, rechargeable batteries, drug delivery, solar cells, and electronics, have also been reported.[6] The most relevant developments in this field over the last years as well as long-term potential applications of inorganic fullerene-like nanoparticles and inorganic nanotubes have been presented in a review by Tenne.[13]

The unidirectional growth of materials to form nanowires or nanotubes has attracted enormous interest in recent years. Because of their many interesting properties (i.e., small dimensions, high anisotropy, and intriguing tube-like structures), carbon nanotubes (CNT) were found to be promising additives to polymeric materials, leading to the enhancement of various properties of the resulting composites.[14−16] However, the fabrication of high-quality composites often requires very pure starting material, good particle dispersion, and strong interaction and adhesion between nanoparticles and polymer matrix. These requirements still pose great difficulties for CNT composites. For these reasons, the synthesis of alternative filler particle types, in

Received: December 6, 2010
Revised: January 19, 2011
Published: March 09, 2011

particular inorganic nanotubes, becomes increasingly important. Recently, INT like-WS_2 are routinely synthesized in large amounts by ApNano Materials, Inc. (NanoMaterials, Ltd.) (http://www.apnano.com).[17] The nanotubes are relatively long with respect to their diameter, and it is this high aspect ratio property that gives them their unique strength and chemical properties. The process does not require a catalyst, and the precursors (tungsten oxide and H_2S or sulfur) are relatively inexpensive. Therefore, the moderate cost of such nanotubes may afford numerous applications in the field of polymer nanocomposites.

In this context, in our previous investigation,[18] we have successfully developed a new family of nanocomposites, which integrated promising molybdenum disulfide nanotubes (MoS_2) in isotactic polypropylene (i.e., the most widely investigated polymer for use in the preparation and application of nanocomposites) by means of the most simple, cost-effective, and ecologically friendly processing way (i.e., melt-processing route). The successful dispersion of INT-MoS_2 induced a remarkable improvement in the thermal and mechanical properties of iPP, without using modifiers or surfactants. The present work is particularly focused on the analysis of the dynamic crystallization behavior of these nanocomposites to better understand the influence of INT-MoS_2 on the crystallization. It is well-known that the properties of a crystalline polymer including the thermodynamic, physical, or mechanical ones depend on the details of the structure and morphology that evolve from the melt. Thus, detailed investigation of the influence of INT-MoS_2 on the crystallization kinetics of iPP would give an insight into the structure−property−performance relationship of such nanocomposites.

2. EXPERIMENTAL SECTION

2.1. Materials and Processing. The polypropylene (PP) used as matrix was an isotactic homopolymer, provided by REPSOL, with a polydispersity of 4.77, an isotacticity of 95%, and a viscosity average molecular weight of 179 000 g/mol. The INT-MoS_2 were provided by NANOTUL (Slovenia) and have been synthesized using $Mo_6S_2I_8$ nanowires as precursor crystals by sulfurization[19] at 1073 K.[20] X-ray fluorescence analysis revealed MoS_2 (99.9%) with some traces of the remained iodine (200 ppm). Several concentrations of INT-MoS_2 (0.1, 0.5, and 1 wt %) were introduced in the iPP matrix by melt-mixing using a microextruder (Thermo-Haake Minilab system) operated at 210 °C and a rotor speed of 150 rpm for 15 min.

2.2. Characterization Techniques. The crystallization behavior of the iPP/INT-MoS_2 nanocomposites was investigated by DSC using a Perkin-Elmer DSC7/Pyris differential scanning calorimeter, calibrated with indium (T_m = 156.6 °C, ΔH_m = 28.45 kJ/kg) and zinc (T_m = 419.47 °C, ΔH_m = 108.37 kJ/kg). The experiments were carried out in a nitrogen atmosphere at a rate flow of 25 mL/min, using approximately 10 mg of sample sealed in aluminum pans. Before the data of crystallization were collected, the samples were heated to 210 °C and held in the molten state for 5 min to eliminate the influence of thermal history. Next, the crystallization of the samples under dynamic conditions was carried out by cooling from 210 to 30 °C at 1, 2, 5, 10, and 20 °C/min. Partial areas, corresponding to a given percentage of the total transformation, were determined from the data points of the exotherm. For the estimation of the crystallinity of the samples, a value of 190 J/g for the melting enthalpy of 100% crystalline iPP was used.[21]

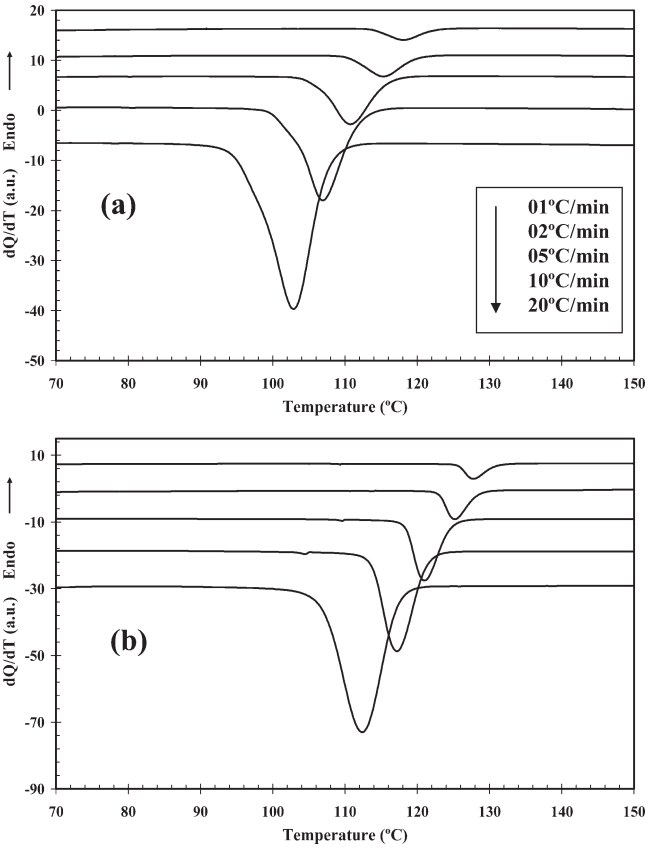

Figure 1. DSC thermograms of dynamic crystallization of (a) iPP and (b) iPP/INT-MoS_2 (1 wt %) obtained at indicated cooling rates.

Small and wide-angle X-ray scattering (SAXS/WAXS) experiments using synchrotron radiation were performed at the A2 beamline of the HASYLAB synchrotron facility (DESY, Hamburg). The experiments were performed with monochromatic X-rays of 0.15 nm wavelength using a germanium single crystal as the dispersing element. The scattering was detected with a linear Gabriel detector. The sample to detector distance of SAXS was 2360 mm, and for WAXS it was 135 mm. The scattering angle of the SAXS pattern was calibrated with the RTT (rat tail tendon), and that of the WAXS profile was calibrated with a PET standard. The maximum of the Lorentz-corrected SAXS diffractograms was used to calculate the long period (L = 1/smax) as a function of the temperature. L represents the sum of the average thickness of the crystal lamellae and of the interlamellar amorphous regions. The methodology used in the dynamic crystallization experiments of the iPP/INT-MoS_2 nanocomposites by SAXS/WAXS was similar to that described for the calorimetric experiments. Measurements were performed with acquisition time of 12 s (wait time = 2 s and read time = 10 s).

3. RESULTS AND DISCUSSION

The crystallization rate of polymers is a very important property from an industrial point of view, as it affects the production time of thermoplastic goods. Crystallization is considered to occur in two steps, which is usually preceded by homogeneous nucleation, heterogeneous nucleation, or self-nucleation and then by growth of the crystal with crystallization time. For a crystallizable polymer, nucleation may be caused by homogeneous or by heterogeneous (impurities, nucleating agent, or others), which can control the structure and physical

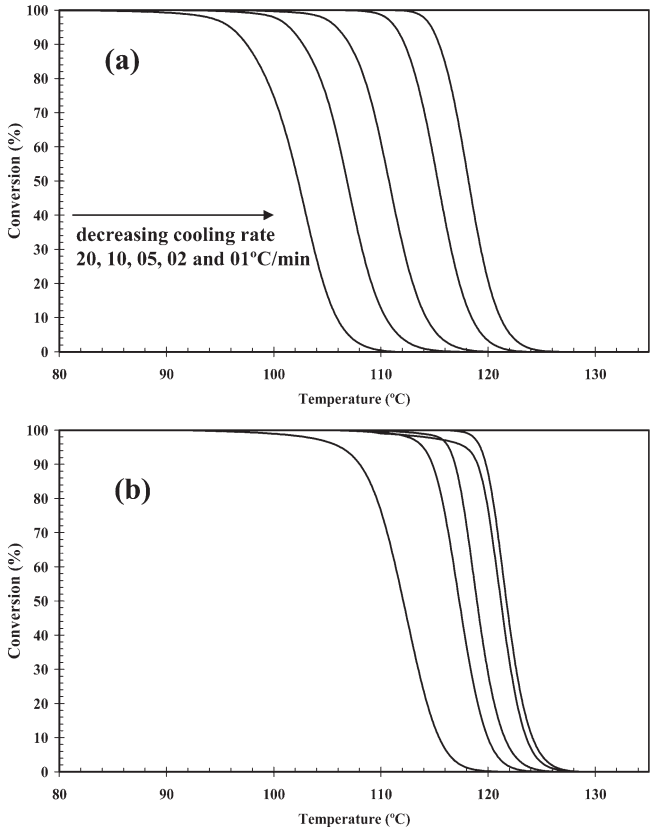

Figure 2. Plots of degree of conversion (x) versus temperature for (a) iPP and (b) iPP/INT-MoS_2 (1 wt %) crystallized nonisothermally at various cooling rates.

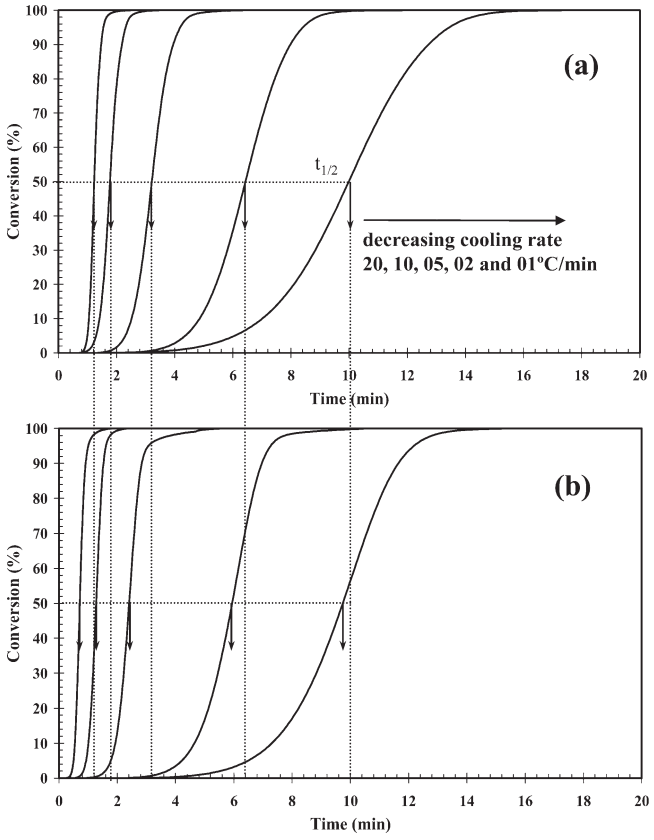

Figure 3. Plots of degree of conversion (x) versus time for (a) iPP and (b) iPP/INT-MoS_2 (1 wt %) crystallized nonisothermally at various cooling rates; the inset is the time needed to reach 50% of crystalline transformation.

properties of polymer. Therefore, overall crystallization behavior of polymers can be analyzed by the observation of the rates of nucleation and growth or the overall rate of crystallization of polymers, which can forecast the relationship between the structures and preparation conditions of the polymers.

It is well-known that the crystallization of polymers releases a significant amount of heat that makes DSC a preferred method for measuring the overall crystallization kinetics. The measured rate of heat release is assumed to be proportional to the macroscopic rate of crystallization:

$$\frac{dQ}{dt} = Q_c \frac{dx}{dt} \tag{1}$$

where Q_c is the measured heat of crystallization. The value of Q_c is calculated by integration of a DSC peak. The values of Q_c can further be used to determine the crystallization rate, dx/dt, as well as the extent of the melt conversion:

$$x(t) = \frac{1}{Q_c}\int_0^t \frac{dQ}{dt}dt \tag{2}$$

The value of $x(t)$ varies from 0 to 1 and represents the degree of conversion. The transformation from temperature to time is performed using a constant cooling rate ϕ:

$$t = \frac{T_0 - T}{\phi} \tag{3}$$

where T is the temperature at time t and T_i is the temperature at the beginning of crystallization. Figure 1 shows the typical

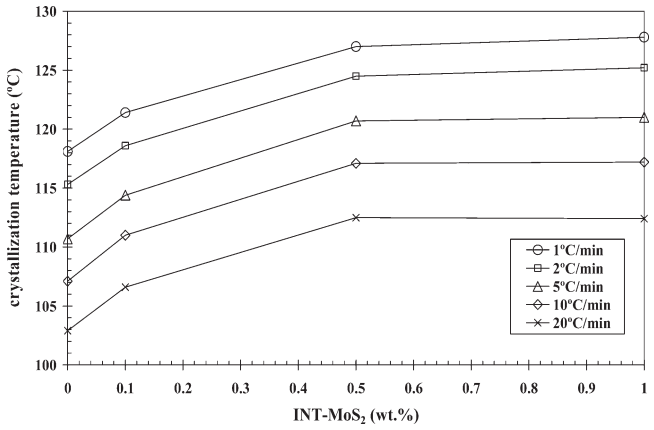

Figure 4. Crystallization temperatures of iPP/INT-MoS_2 nanocomposites obtained at various cooling rates.

dynamic crystallization thermograms obtained at various cooling rates for neat iPP and the iPP/INT-MoS_2 nanocomposite with an INT-MoS_2 content of 1 wt %. In both cases, the peak temperature (T_p), which corresponds to the maximum crystallization rate, shifts to lower temperature with increasing cooling rate. It is also seen the lower is the cooling rate, the earlier the crystallization starts. On the other hand, Figure 2 presents the crystallization fraction or conversion as function of temperature. According to eq 3, the value to T on the x-axis in Figure 2 can be transformed into crystallization time as shown in Figure 3. The

dx.doi.org/10.1021/jp1115788 |J. Phys. Chem. B 2011, 115, 2850–2856

lower is the cooling rate, the larger is the temperature (time) range at which the crystallization occurs, which indicates that the transformation is controlled by nucleation. In addition, all curves have the same S (or reversed S) shape, indicating that only the retardation effect of cooling rate on the crystallization is observed in these curves. However, the most obvious result was the influence of INT-MoS_2 on, for example, the crystallization temperature (T_p) of iPP for a particular cooling rate. The crystallization temperature of iPP increases with the incorporation of INT-MoS_2 at all cooling rates as shown in Figure 4. This effect was clearly observed to be a function of composition, manifesting a significant increase of around 4 °C of this parameter at a cooling rate of 10 °C/min. At higher INT-MoS_2 concentrations, the value of T_p for iPP continues to rise and tends to stabilize for the highest concentrations of 0.5 and 1%, where increments of around 10 °C in the value of T_p were registered. In the same way, the crystallinity increases up to 14% with the IF-MoS_2 content, from a average value of 50% for iPP, to values of 54%, 57%, and 56% for the nanocomposites with 0.1, 0.5, and 1 wt %, respectively. The increase in the crystallization temperature and crystallinity of iPP with increasing INT-MoS_2 content suggests that INT-MoS_2 can effectively act as nucleating agent in iPP/INT-MoS_2 nanocomposites. It is generally accepted that the addition of nanoparticles into the polymer matrix favors heterogeneous nucleation and thus is expected to make the molecular chains of polymer matrix easier to crystallize and increase the crystallization rate of composites in contrast to that of neat polymer (e.g., increase of peak crystallization temperature of polymer matrix). Such a result has already been found with other nanocomposite systems, such as nylon-6/clay,[22] PEN/Silica,[23] PEN/MWCNT,[24] iPP/SiO_2,[25] iPP/IF-WS_2,[7] nylon-6/SWNT,[26] iPP/MCWNT,[27] and iPP/C_3N_4.[28] However, in some specific systems, we have observed that the incorporation of IF-WS_2 or modified SWCNTs induces a variation of the crystallization behavior of polymeric materials like PEEK or PPS with increasing nanofiller content (i.e., a drastic change from promotion to retardation and vice versa[10,12,29]).

To quantitatively describe the evolution of crystallinity during dynamic crystallization, a number of models have been proposed in the literature. In this investigation, the Lui method was tested.

3.1. Combined Ozawa−Avrami Approach. A convenient approach adopted here for describing nonisothermal crystallization was the Liu model.[30] By combining the Avrami[31] and Ozawa[32] equations, a new treatment was proposed and proved to be suitable and convenient to handle the nonisothermal crystallization of poly(aryl ether ether ketone ketone) (PEEKK) as well as in other recently reported studies on PPS/IF-WS_2[10,11] and iPP/C_3N_4.[28] As the degree of conversion (x) was related to the cooling rate ϕ and the crystallization time t (or temperature T), the relation between ϕ and t could be defined for a given degree of conversion. Consequently, a new kinetic equation for dynamic crystallization was derived:

$$\ln \phi = \ln f(T) - \alpha \ln t \tag{4}$$

where $f(T) = [k'(T)/k]^{1/m}$ refers to the value of cooling rate chosen at unit crystallization time, when the system has a certain degree of crystallinity, and α is the ratio of the Avrami exponents to Ozawa exponents (i.e., $\alpha = n/m$). According to eq 4, at a given degree of conversion, the plot of $\ln \phi$ versus $\ln t$ gives a gives a series of lines as can be seen in Figure 5. The good linearity of the plots verifies the advantage of the combined approach applied in this case. The values of $f(T)$ and α are listed in Table 1, from which one can

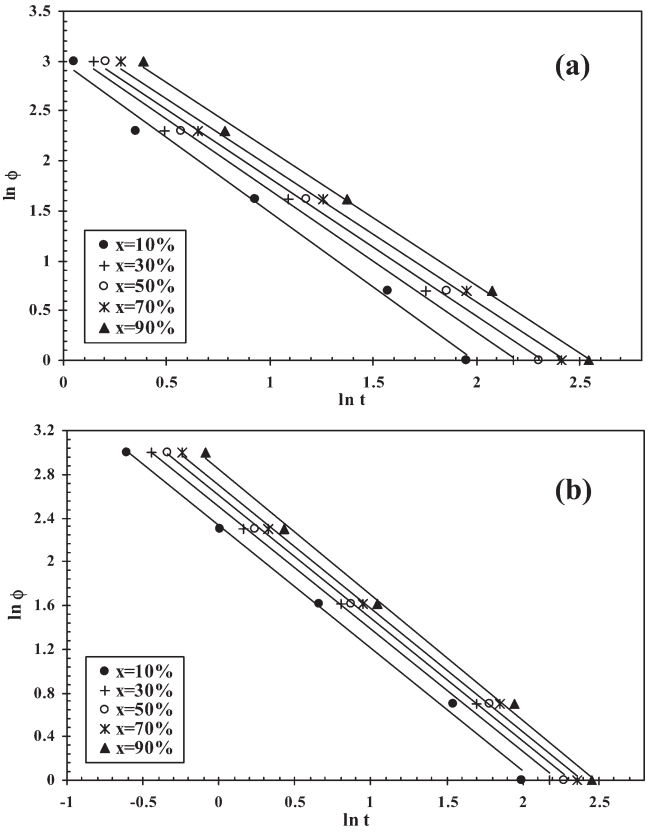

Figure 5. Liu plots of the dynamic crystallization of (a) iPP and (b) iPP/INT-MoS_2 (1 wt %).

read that the values of $f(T)$ increase systematically with increasing relative crystallinity, indicating that at unit crystallization time, a higher cooling rate should be required to obtain a higher degree of crystallinity, while the values of the parameter a are almost constant (e.g., $\alpha_{iPP} = 1.35-1.50$ and $\alpha_{1wt\%\ INT\text{-}MoS2} = 1.12-1.15$). However, the most important observation was the influence of INT-MoS_2 concentration on the value of $f(T)$ of iPP for a particular degree of conversion. The value of $f(T)$ for neat iPP is higher than that for nanocomposites, which implies that the composites require a lower heating rate to approach an identical degree of crystalline transformation. In other words, the crystallization rate of the nanocomposites is lower than that of neat iPP. This result suggests that the presence of INT-MoS_2 acts as nucleating sites for the dynamic crystallization process of iPP.[23]

3.2. Nucleation Ability. Dobreva and Gutzow[33,34] developed a simple method for calculating the nucleation activity of foreign substrates in polymer melt. Nucleation activity (φ) is a factor by which the work of three-dimensional nucleation decreases with the addition of a foreign substrate. If the foreign substrate is extremely active, φ approaches 0, while for inert particles, φ approaches 1. For homogeneous nucleation from a melt near the melting temperature, the cooling rates can be written as:

$$\ln \phi = A - \frac{B}{\Delta T_p^2} \tag{5}$$

while for the heterogeneous case:

$$\ln \phi = A - \frac{B^*}{\Delta T_p^2} \tag{6}$$

dx.doi.org/10.1021/jp1115788 |J. Phys. Chem. B 2011, 115, 2850–2856

Table 1. Values of α and $f(T)$ versus Conversion (x) Based on the Liu Model for iPP/INT-MoS_2 Nanocomposites

INT-MoS_2 content (wt %)	x (%)	α	$f(T)$	φ^a	ΔE (kJ/mol)^b	ΔE (kJ/mol)^c
0.0	10	1.50	19.60	1.00	−246.6	−240.2
	30	1.42	22.70			
	50	1.38	24.69			
	70	1.36	27.06			
	90	1.35	31.65			
0.1	10	1.21	11.28	0.96	−259.9	−253.4
	30	1.19	13.41			
	50	1.18	14.80			
	70	1.18	16.04			
	90	1.18	18.08			
0.5	10	1.18	09.55	0.75	−271.5	−268.0
	30	1.18	11.55			
	50	1.19	12.96			
	70	1.20	14.53			
	90	1.23	17.25			
1.0	10	1.13	10.29	0.69	−255.8	−249.3
	30	1.12	12.22			
	50	1.12	13.50			
	70	1.13	14.90			
	90	1.15	17.22			

[a] Nucleation activity calculated using Dovreba's equation. [b] Effective energy barrier calculated using Kissinger's equation. [c] Effective energy barrier calculated using Takhor's equation.

$$\varphi = \frac{B^*}{B} \tag{7}$$

where ϕ is the cooling rate, A is a constant, and ΔT_p is the degree of supercooling, that is, $\Delta T_p = T_m - T_p$, and T_p is the temperature corresponding to the peak temperature of the DSC crystallization curves. B is a parameter that can be calculated from the following equation:

$$B = \frac{\omega\sigma^3 V_m^2}{3nk_B T_m^0 \Delta S_m^2} \tag{8}$$

where ω is a geometrical factor; σ is the specific energy, V_m is the molar volume of the crystallizing substance, n is the Avrami exponent, ΔS_m is the entropy of melting, k_B is the Boltzmann constant, and T_m^0 is the infinite crystal melting temperature. In Figure 6, eqs 5 and 6 are represented for neat iPP and its nanocomposites, considering a value of 196 °C for the thermodynamic equilibrium melting temperature of iPP.[8] From the slopes of the linear plots, the values of B and B^* can be calculated for iPP and the nanocomposites, respectively, and the results of all iPP/INT-MoS_2 nanocomposites are listed in Table 1. As can be seen, the addition of INT-MoS_2 cause a reduction of φ, which reaches a value of 0.69 for a concentration of 1 wt % of INT-MoS_2, indicating that INT-MoS_2 was acting effectively as a nucleating agent in the iPP matrix. The higher value of INT-MoS_2 obtained at 1wt % is above the values reported in the literature for other fillers including nanometric silica particles (e.g., 0.94[25]) and carbon nitrides C_3N_4 (e.g., 0.82[28]) and is comparable to MWCNTs.[27]

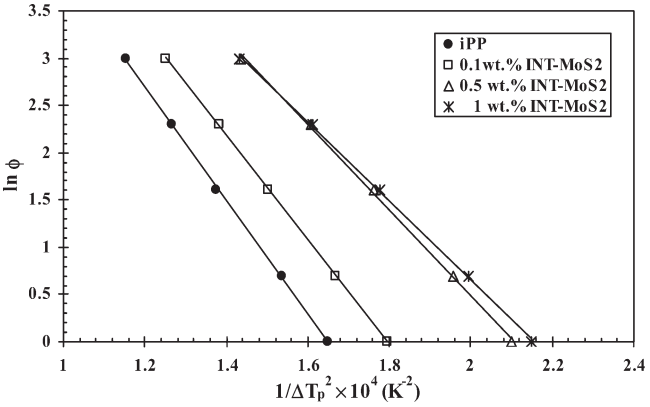

Figure 6. Dobreva plots for evaluating nucleation activity of INT-MoS_2 in iPP/INT-MoS_2 nanocomposites.

3.3. Effective Energy Barrier. Crystallization activation energy, or effective energy barrier ΔE, can be used to estimate the growth ability of the chain segments. Considering the variation of the peak temperature T_p with the cooling rate ϕ, ΔE could be determined as follows:

(1) Kissinger model[35]

$$\ln\left(\frac{\phi}{T_p^2}\right) = \text{constant} - \frac{\Delta E}{RT_p} \tag{9}$$

(2) Takhor model[36]

$$\ln(\phi) = \text{constant} - \frac{\Delta E}{RT_p} \tag{10}$$

where R is the universal gas constant. Figure 7 shows an example of the plots of the Kissinger and Takhor models. Linearity of these plots was the most popular testing methods for the validity of the calculations of the effective energy barrier, and the results of all iPP/INT-MoS_2 nanocomposites are listed in Table 1. As can be seen, the isokinetic models of Kissinger and Takhor based on one experimental point from each curve (the maximum of the crystallization peak) all showed that the nanocomposites had lower values of ΔE than of iPP. The addition of INT-MoS_2 caused a decrease in the ΔE, which made the molecular chains of iPP easier to crystallize, and increased the crystallization rates due to the nucleation activity of the INT-MoS_2.

3.4. Crystal Morphology and Structure. Understanding the structure of new polymer nanocomposites requires advanced experimental techniques. As an example, electromagnetic radiation can be used to obtain information about materials whose dimensions are on the same order of magnitude as the radiation wavelength. Scattering of X-rays is caused by differences in electron density. Because the larger is the diffraction angle, the smaller is the length scale probed, wide-angle X-ray diffraction (WAXD) is used to determine the crystal structure on the atomic length scale, while small-angle X-ray scattering (SAXS) is used to explore the microstructure at the nanometer scale. Figure 8 shows the in situ WAXS experiments of an iPP nanocomposite containing 1 wt % of INT-MoS_2 using synchrotron radiation. Under the dynamic crystallization conditions, iPP crystallized in the α or monoclinic form. The WAXS diffractograms of iPP/INT-MoS_2 nanocomposites only present reflections associated

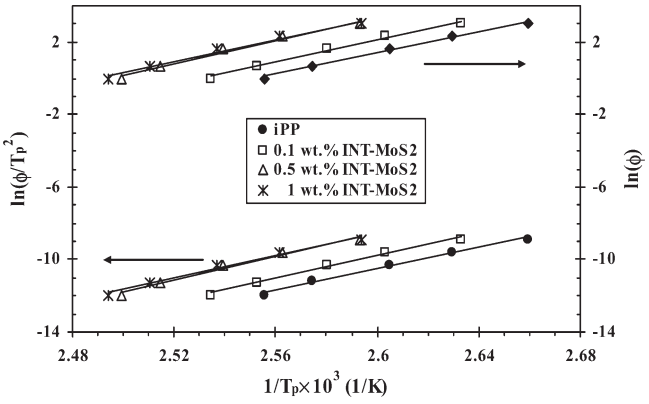

Figure 7. Kissinger and Takhor plots for evaluating the effective energy barrier of iPP/INT-MoS_2 nanocomposites.

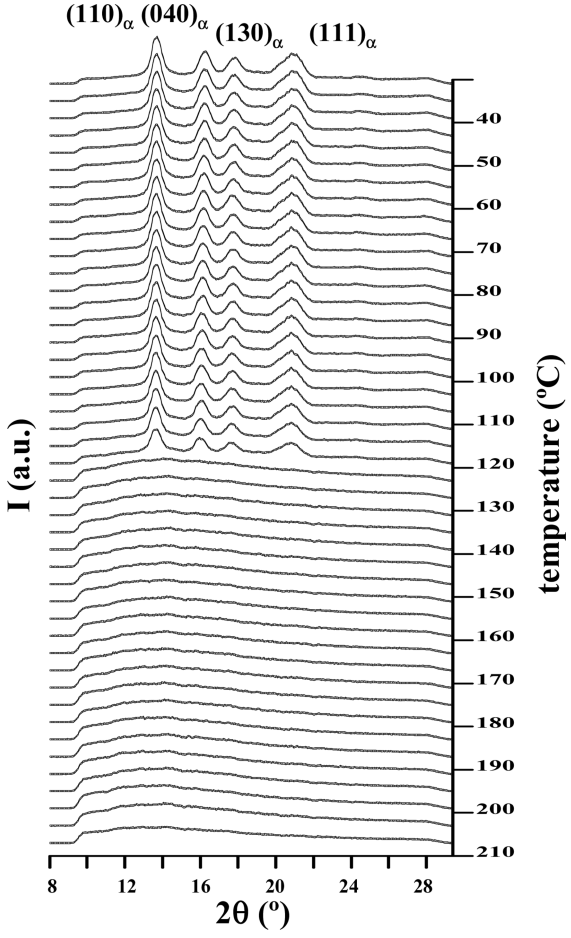

Figure 8. WAXS diffractograms of iPP/INT-MoS_2 (1 wt %) obtained during cooling from the melt to room temperature at 10 °C/min.

with the crystalline planes characteristic of the monoclinic polymorph of iPP.[7] No other crystalline forms of iPP were detected during cooling of the nanocomposites. On the other hand, the dependence of the lamellar structure of iPP on composition can also be obtained from the SAXS experiments of the nanocomposites during the crystallization from the melt at 10 °C/min. As an example, the results obtained at room temperature indicated that the addition of INT-MoS_2 caused no appreciable change in the long period (L) of iPP (i.e., ∼15 nm). From the results of the L data, the possible role of the INT-MoS_2 in the variation of thickness of the crystal lamellae of iPP can be investigated. As noted previously, L can be considered as the sum of the average thickness of the crystal lamellae and of the interlamellar amorphous regions. In addition, the parameter L and the crystallinity can also be used as a simple approximation to calculate the average thickness of the crystal lamellae of iPP. Therefore, the increase in crystallinity of the composites, observed from the DSC data during the dynamic crystallization, could be connected to the increase of the size of the crystallites of iPP in the iPP/INT-MoS_2 nanocomposites.

4. CONCLUSION

On the basis of the experimental and theoretical analyses, the study of the dynamic crystallization kinetics of iPP/INT-MoS_2 nanocomposites provides a picture describing the transformation of iPP molecules from the nonordered state to the ordered state. The analysis of the influence of INT-MoS_2 on the dynamic crystallization kinetics of iPP shows a significant dependence on INT-MoS_2 content and cooling rate. The crystallization temperature for the iPP/INT-MoS_2 nanocomposites decreased with increasing cooling rate for a given INT-MoS_2 content and increased with INT-MoS_2 content for a given cooling rate. The incorporation of INT-MoS_2 induces an increase in the crystallinity, while maintaining the monoclinic crystalline structure of iPP. On the other hand, the method developed by Liu at al., which combines the theories of Avrami and Ozawa, was successful in describing the crystallization of iPP/INT-MoS_2 nanocomposites. The parameter $f(T)$, which has physical and practical significance, increased with INT-MoS_2, indicating that the crystallization rate increased with the INT-MoS_2 content as compared to iPP. Therefore, INT-MoS_2 acted as nucleation agents in the iPP matrix, and the nucleating activities, which indicated the contribution of the nanofiller to the polymer matrix, revealed that INT-MoS_2 has a remarkable nucleation effect on iPP. Finally, the energy barrier governing the dynamic crystallization based on Kissinger and Takhor models all showed iPP/INT-MoS_2 nanocomposite had a lower value of ΔE than of neat iPP, which indicated the nanocomposite has a faster crystallization rate.

AUTHOR INFORMATION

Corresponding Author

*E-mail: mnaffakh@ictp.csic.es.

ACKNOWLEDGMENT

M.N. would like to express his sincere thanks to the Consejo Superior de Investigaciones Cientificas (CSIC) for postdoctoral contract (I3PDR-6-02), financed by the European Social Fund, the European Commission for the X-ray synchrotron experiments performed at the Soft Condensed Matter A2 beamline at HASYLAB (DESY-Hamburg, I-20100101 EC). M.R. would like to thank Janez Jelenc for help in the synthesis of MoS_2 nanotubes. Work was partially financed by the Ministry of Higher Education, Science, and Technology of the Republic of Slovenia and by the FOREMOST project of the European Union 6-th Framework Program under contract NMP3-CT-2005-515840.

REFERENCES

(1) Kroto, H. W.; Heath, J. R.; O'Brien, S. C.; Curl, R. F.; Smalley, R. E. *Nature* **1985**, *318*, 162–163.
(2) Iijima, S. *Nature* **1991**, *354*, 56–58.
(3) Tenne, R.; Margulis, L.; Genut, M.; Hodes, G. *Nature* **1992**, *360*, 444–445.
(4) Margulis, L.; Salitra, G.; Tenne, R.; Talianker, M. *Nature* **1993**, *365*, 113–14.
(5) Remškar, M. *Adv. Mater.* **2004**, *16*, 1497–1502.
(6) Tenne, R. *Nat. Nanotechnol.* **2006**, *1*, 103–111.
(7) Naffakh, M.; Martín, Z.; Fanegas, N.; Marco, C.; Gómez, M. A.; Jiménez, I. *J. Polym. Sci., Part B: Polym. Phys.* **2007**, *45*, 2309–2321.
(8) Naffakh, M.; Martín, Z.; Marco, C.; Gómez, M. A.; Jiménez, I. *Thermochim. Acta* **2008**, *472*, 11–16.
(9) Naffakh, M.; Marco, C.; Gómez, M. A.; Jiménez, I. *J. Phys. Chem. B* **2008**, *112*, 14819–14828.
(10) Naffakh, M.; Marco, C.; Gómez, M. A.; Jiménez, I. *J. Phys. Chem. B* **2009**, *113*, 7107–7115.
(11) Naffakh, M.; Marco, C.; Gómez, M. A.; Gómez-Herrero, J.; Jiménez, I. *J. Phys. Chem. B* **2009**, *113*, 10104–10111.
(12) Naffakh, M.; Diez-Pascual, A. M.; Marco, C.; Gómez, M. A.; Jiménez, I. *J. Phys. Chem. B* **2010**, *114*, 11444–11453.
(13) Tenne, R.; Redlich, M. *Chem. Soc. Rev.* **2010**, *39*, 1423–1434.
(14) Moniruzzaman, M.; Winey, K. I. *Macromolecules* **2006**, *39*, 5194–5205.
(15) Maser, W. K.; Benito, A. M.; Castel, P.; Sainz, R.; Martínez, M. T.; Naffakh, M.; Marco, C.; Ellis, G.; Gómez, M. A. In *Nanostructured Materials for Advanced Technological Applications*; Reithmaier, J. P., Petkov, P., Kulisch, W., Popov, C., Eds.; NATO Science for Peace and Security Series − B: Physics and Biophysics ; Springer: Dordrecht, the Netherlands, 2009; p 181.
(16) Bose, S.; Khare, R. A.; Moldenaers, P. *Polymer* **2010**, *51*, 975–993.
(17) Zak, A.; Sallacan-Ecker, L.; Margolin, A.; Genut, M.; Tenne, R. *Nano* **2009**, *4*, 91–98.
(18) Naffakh, M.; Remškar, M.; Marco, C.; Gómez, M. A.; Jiménez, I. *J. Mater. Chem.* **2011**, *21*, 3574−3578.
(19) Remskar, M.; Mrzel, A.; Virsek, M.; Jesih, A. *Adv. Mater.* **2007**, *19*, 4276–4278.
(20) Remskar, M.; Virsek, M.; Mrzel, A. *Appl. Phys. Lett.* **2009**, *95*, 133122.
(21) Li, J. X.; Cheung, W. L.; Demin, J. *Polymer* **1999**, *40*, 1219–1222.
(22) Devaux, E.; Bourbigot, S.; El Achari, A. *J. Appl. Polym. Sci.* **2002**, *86*, 2416–23.
(23) Kim, S. H.; Ahn, S. H.; Hirai, T. *Polymer* **2003**, *44*, 5625–34.
(24) Kim, J. Y.; Park, H. S.; Kim, S. H. *Polymer* **2006**, *47*, 1379–89.
(25) Papageorgiou, G. Z.; Achilias, D. S.; Bikiaris, D. N.; Karayannidis, G. P. *Thermochim. Acta* **2005**, *427*, 117–28.
(26) Naffakh, M.; Marco, C.; Gómez, M. A.; Ellis, G.; Maser, W. K.; Benito, A.; Martínez, M. T. *J. Nanosci. Nanotechnol.* **2009**, *9*, 6120–6126.
(27) Marco, C.; Naffakh, M.; Gómez, M. A.; Santoro, G.; Ellis, G. *Polym. Compos.* **2011**, *32*, 324–333.
(28) Naffakh, M.; López, V.; Zamora, F.; Gómez, M. A. *Soft Matter* **2010**, *8*, 407–425.
(29) Díez-Pascual, A. M.; Naffakh, M.; Gónzalez-Domínguez, J. M.; Martínez-Rubi, Y.; Ansón, A.; Martínez, M. T.; Simard, B.; Gómez, M. A. *Carbon* **2010**, *48*, 3485–3499.
(30) Liu, T.; Mo, Z.; Wang, S.; Zhang, H. *Polym. Eng. Sci.* **1997**, *37*, 568–575.
(31) Avrami, M. *J. Chem. Phys.* **1939**, *7*, 1103–1112; *J. Chem. Phys.* **1940**, *8*, 212–224; *J. Chem. Phys.* **1941**, *9*, 177–184.
(32) Ozawa, T. *Polymer* **1971**, *12*, 150–158.
(33) Dobreva, A.; Gutzow, I. *J. Non-Cryst. Solids* **1993**, *162*, 1–12.
(34) Dobreva, A.; Gutzow, I. *J. Non-Cryst. Solids* **1993**, *162*, 13–25.
(35) Kissinger, H. E. *J. Res. Natl. Bur. Stand. (U.S.)* **1956**, *57*, 217–221.
(36) Takhor, R. L. *Advances in Nucleation and Crystallization of Glasses*; American Ceramics Society: Columbus, OH, 1971; pp 166−172.